Materials & Design 208 (2021) 109944

Contents lists available at ScienceDirect

Materials & Design

journal homepage: www.elsevier.com/locate/matdes

Controlled synthesis of mussel-inspired Ag nanoparticle coatings with demonstrated *in vitro* and *in vivo* antibacterial properties

Xiaowei Wang [a], Kehui Xu [a], Wendi Cui [a], Xi Yang [a], Manfred F. Maitz [b], Wei Li [a], Xiangyang Li [a], Jialong Chen [a]

[a] Stomatologic Hospital and College, Anhui Medical University, Key Laboratory of Oral Diseases Research of Anhui Province, Hefei, Anhui 230032, China
[b] Max Bergmann Center of Biomaterials, Leibniz Institute of Polymer Research Dresden, Hohe Strasse 6, 01069 Dresden, Germany

HIGHLIGHTS

- pH is as important as the feeding Ag^+ concentration to determine the AgNPs formation.
- Firstly proposed alkaline environment was favorable for AgNPs formation.
- pH 10/0.1 exhibits dramatically antibacterial property and osteogenesis.

GRAPHICAL ABSTRACT

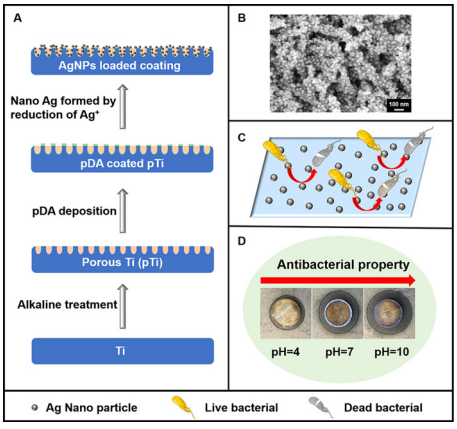

ARTICLE INFO

Article history:
Received 21 February 2021
Revised 28 May 2021
Accepted 27 June 2021
Available online 29 June 2021

Keywords:
AgNPs
Osteogenesis
Antibacterial
pH
Mineralization

ABSTRACT

The *in-situ* formation of silver nanoparticles (AgNPs) via dopamine-reduction of Ag^+ has been widely utilized for titanium implants to introduce antibacterial properties. In previous studies, the preparation of AgNPs has focused on controlling the feeding concentrations, while the pH of the reaction solution was ignored. Herein, we systematically determined the influence of various pH (4, 7, 10) and Ag^+ concentrations (0.01, 0.1 mg/mL) on the AgNPs formation, followed by the evaluation of the antibacterial properties *in vitro* and *in vivo*. The results revealed that an alkaline environment was favourable for AgNP formation and resulted in more particles. Although the AgNPs bearing Ti had lower biocompatibilities, it was significantly improved after 7 days of mineralization in simulated body fluid. The outstanding antibacterial property of the AgNPs was well maintained after one day and seven days of implantation. Moreover, 3D micro-CT modelling showed that the pH 10/0.1 group exhibited remarkable osteogenesis, which may be due to their strong antibacterial properties and ability to promote mineralization. Therefore, we have demonstrated that the solution pH was as important as the feeding Ag^+ concentration in determining AgNP formation, and it has paved the way for developing various AgNP-loaded surfaces that could meet different antibacterial needs.

1. Introduction

Biocompatible titanium (Ti) and its alloys are widely used in the repair of hard tissues due to their desirable mechanical and

E-mail addresses: 453951372@qq.com (W. Li), hlxiangyang@163.com (X. Li), jialong_dt@126.com (J. Chen)

https://doi.org/10.1016/j.matdes.2021.109944
0264-1275/

biomedical properties [1]. However, a major limitation of these implants is the possibility of failure due to infections, which often cause serious harm and may require re-hospitalization, re-operations and high economic costs and can even lead to death [2–4]. Moreover, a tenacious microbe biofilm can form on the surface and cause serious postoperative implant-associated infections, which are very resistant to therapeutic approaches [5–7]. It has been reported that 0.5–3.0% and up to 8% of primary and total hip replacements, respectively, have failed due to bacterial infection [8]. Therefore, considering the interaction between bacteria and biological materials is imperative when designing and manufacturing the next generation of implants.

Clinically treating infections relies on antibiotics, which are limited by the increase in antibiotic-resistant strains (e.g., methicillin-resistant *Staphylococcus aureus*, MRSA) and their narrow-spectrum activity [9–11]. Surface modifications, which give the implant antibacterial properties, have emerged as candidates to exert antibacterial effects in situ, and they may reduce the use of antibiotics [12–15]. The use of silver nanoparticles (AgNPs), which have outstanding antimicrobial and anti-biofilm properties, has been noted as an alternative strategy to combat bacterial biofilms [16]. They have received extensive attention due to their broad-spectrum antibacterial activity and favourable stability that occurs without the development of drug resistance [17–19]. Various methods have been developed to incorporate Ag nanoparticles onto Ti implants, such as sputter deposition [20], photoreduction [21], plasma immersion ion implantation [22], and reduction by polyphenols or catecholamines [23,24].

Dopamine (DA) has attracted enormous interest in recent years due to the formation of mussel-inspired adhesive coatings [25–27]. DA forms a stable coating on various substrates and serves as a versatile secondary reaction platform through a simple self-polymerization to poly-dopamine (pDA) in a one-pot approach [28,29]. Among the various secondary reactions initiated by pDA, the reaction that reduces and immobilizes metal ions in situ is able to facilitate the formation of surfaces with metal nanoparticles [30,31]. Many researchers, including our group, have attempted to utilize the pDA coating for in situ generation of AgNPs to yield antibacterial bioimplants [32,33]. In 2011, Messersmith's group fabricated an AgNP-loaded pDA coating on polycarbonate, which showed durable antibacterial activity and 7 days of sustained silver release [34]. Yajie Xie et al. clarified that the chelation between pDA and Ag^+ is the critical factor for Ag stability and its continuous antibacterial properties [35]. However, although AgNPs possess outstanding antibacterial properties, their toxicity cannot be ignored [36].

To date, considerable effort has been made to balance antibacterial properties and toxicity by controlling the feeding Ag^+ concentration [37,38]. However, the pH of the Ag^+-containing solution, another key factor in AgNP generation, has not receive further attention. pH plays a significant role in AgNP formation and influences the particle amount and size. It has been reported that smaller Ag particles with larger specific areas exert better bactericidal effects [39]. Additionally, morphology and size are closely related to pH and influence the release rate of Ag^+ and its activity against biofilms. These properties may synthetically impact the equilibrium between toxicity and cytocompatibility [40,41]. As previous work showed, there is an optimal amount and size of AgNPs, which lessens its toxicity to cells and tissue [42]. Therefore, regulating the pH and feeding concentration of Ag^+ is critical for optimizing the properties of AgNP-bearing surfaces, but only a few studies have comprehensively analysed both the pH and Ag^+ feeding concentrations in the AgNP formation system. Evaluating the biology combined with the underlying mechanisms would also be indispensable.

Antibacterial demands vary among different patients and different stages of implant integration; therefore, the adaptation of a bioimplant to meet physiological demands is essential [43–46]. For the initial implant stage, stronger antibacterial activity is needed, and in the later post-implantation period, tissue repair is more important. Hence, to adapt the antibacterial requirements of different cases, AgNP-loaded surfaces with diverse amounts and sizes of AgNPs are needed, and these variables depends on the reaction conditions, which include the pH and Ag^+ feeding concentration.

In this study, different AgNP-loaded surfaces were prepared on pDA-modified porous titanium by altering the concentration and pH of the silver nitrate solution. After systematic *in vitro* and *in vivo* evaluations, we confirmed that the solution pH was another vital factor which is as important as the Ag^+ feeding concentration in determining AgNP formation and that various AgNP-loaded surfaces were fabricated successfully to meet different antibacterial demands different implant stage.

2. Results and discussion

2.1. Characterization of AgNPs loaded coatings

AgNP-loaded coatings were characterized on the widely used osteosynthesis material titanium. Titanium was alkali-treated to prepare porous titanium (pTi) to improve cell adhesion. The porous titanium was immersed for 24 h in a 0.25 mg/mL alkaline dopamine solution for surface functionalization. Finally, AgNPs were prepared on pDA-functionalized porous titanium by reducing Ag^+ in silver nitrate. To investigate the influence of pH and the feeding concentration of silver nitrate on AgNP generation, different pH and feeding concentrations were applied, which included pH 4/0.01, pH 4/0.1, pH 7/0.01, pH 7/0.1, pH 10/0.01, and pH 10/0.1.

Water contact angles (WCAs) were determined to check the wettability of different samples. As Fig. 1(A) shows, the WCA of pTi was significantly reduced from 64.7° to 10.0 ± 0.5° compared to that of polished Ti since the alkali treatment made the surface porous and rich in hydroxyl groups. It increased to 33.7 ± 7.2° after undergoing functionalization with polydopamine. With the loading of AgNPs, the hydrophilicity of each group increased, which may be due to the change in surface energy and morphology during AgNP formation.

As AgNPs are the main functional unit in these coatings, and the amount and state of Ag on the surface are important. To determine the chemical states and elemental depth profiles of the AgNPs formed on pTi-DA, these coatings were analysed by XPS, and the results are presented in Fig. 1(B) and Fig. S1. The Ag doublet at 368.2 eV corresponds to Ag and Ag_2O, and the peak at 374.2 corresponds to Ag 3d3, and these both indicate AgNP formation. As shown in Fig. 1(B), both the pH and the feeding concentration of the silver nitrate solution significantly influenced AgNP formation on the surface. More AgNPs were formed as the pH and feeding concentration of silver nitrate increased, which suggests that the antimicrobial activity of these coatings may also be modified by these parameters. To further determine the type of Ag on the surface, surface plasmon resonance spectroscopy was performed, which is a standard tool for measuring the adsorption type of nanoparticles. SPR peaks (Fig. S2) at λ_{max} = 400 and 460 nm were observed, indicating that AgNPs had formed [47]. The absorbance intensity of AgNP solutions increased with increasing pH, which indicated that there were increasing numbers of AgNPs. XPS and SPR revealed the generation of AgNPs, and QCM-D was used to determine the mode of AgNP formation. Once silver nitrate was added, the resonance frequency for the pH 10/0.01 and pH 10/0.1 solutions rapidly dropped, while the other groups began to oscillate. The drop and oscillation may be attributed to the stability of the newly synthesised AgNPs, which confirms that the reaction

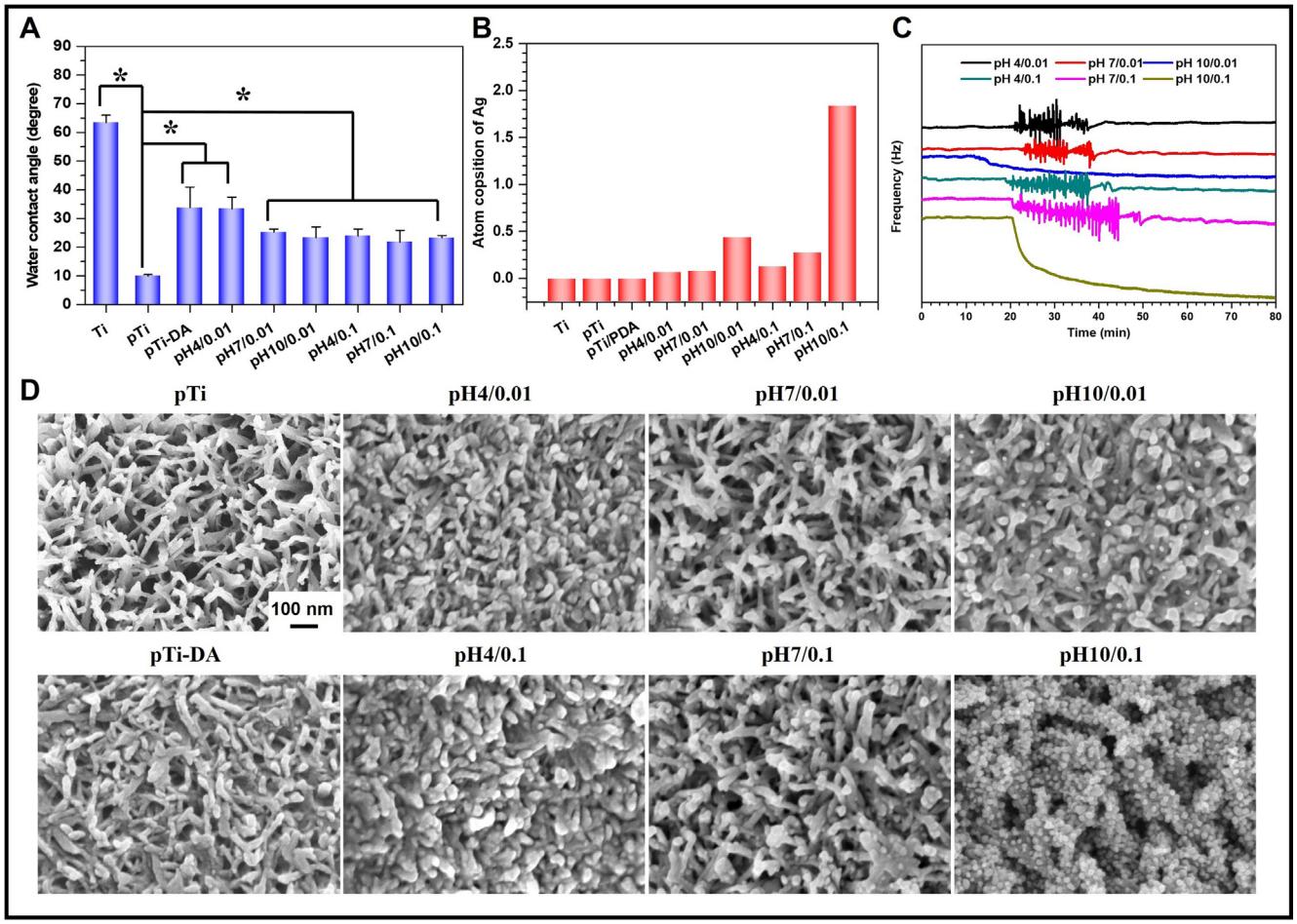

Fig. 1. Characterization of AgNPs loaded coatings. (A) Water contact angles of Ti, porous Ti, pDA-coated porous Ti and AgNP-modified porous Ti. (B) Atom composition of Ag on Ti, porous Ti, pDA-coated porous Ti and AgNP-modified porous Ti determined by XPS. (C) The result of QCM-D, which shows the frequency and amount change of AgNPs formed on pDA-coated porous Ti. (D) SEM images of the surfaces.

was stable under alkaline conditions, and more AgNPs were formed when the pH increased to 10.

The surface morphologies of the Ti, pTi, pTi-DA, pH 4/0.01, pH 4/0.1, pH 7/0.01, pH 7/0.1, pH 10/0.01, and pH 10/0.1 samples are shown in Fig. 1(D). Compared to the bare Ti, the NaOH-treated Ti presented a uniform microporous morphology with multiple struts. Some of these pores were filled or bridged by the pDA coating. Treatment with silver nitrate at different concentrations and pH values caused major changes in the surface morphology. As Fig. 1(D) shows, no obvious difference was observed on the surface of pH 4/0.01 and pH 4/0.1 compared to pTi-DA. With the increased pH of the silver nitrate solution (pH 7/0.01, pH 7/0.1), evenly distributed nano-silver was observed. As the pH increased to 10, the particles displayed spherical and irregular shapes and were evenly dispersed on the surface. It can be concluded that nano-silver particles successfully form on pDA-modified pTi, and their amount and shape can be adjusted by the pH and feed concentration of the silver nitrate solution.

2.2. Antibacterial assessment

To evaluate the antibacterial properties of the AgNP-loaded coatings, bacterial counting, inhibition zone, and live and dead bacterial assays were carried out. Bacterial counting and the zone inhibition test showed that bacteria could not proliferate on the AgNP-loaded coatings. Live/dead staining and replating showed that bacteria were killed rather than just having their proliferation inhibited [6,48].

First, we placed various samples in inoculum with graded bacterial concentrations. As shown in supplementary Fig. S3, after co-incubation for 6 h, the AgNP-loaded coatings significantly inhibited bacterial proliferation and maintained a clear inoculum. The antibacterial activity, determined as the clarity of the inoculum, was dependent on the amount of AgNPs in the samples of the pH 7/0.1, pH 10/0.01, and pH 10/0.1 groups that showed the best antibacterial properties.

Antibacterial activity is essential for an implant and can be investigated via zone of inhibition (ZOI) tests and optical density measurements. The samples were incubated with bacterial suspensions for 24 h, and the quantity of bacteria was monitored by measuring the optical density at 660 nm (OD 660). As shown in Fig. S4, the Ag-free samples Ti, pTi, and pTi-DA did not present antibacterial activity against *S. aureus* when the OD value exceeded 0.5 after 24 h of culture. Clear and translucent inhibition zones (black circles) of different sizes (white numbers) were observed around all nanosilver-modified samples except for pH 4/0.01, indicating that they can inhibit growth or directly kill microbes around them to varying degrees. The antibacterial properties increased with increasing pH during the coating preparation, confirming the results of the local antibacterial tests.

To simulate the physiological process after implants are placed within the body, samples were immersed in simulated body fluid

(SBF) for certain periods of time, and the mineralized surfaces were again tested in bacterial suspensions and ZOI tests. After two days of immersion in SBF, the mineralized M2-pH 7/0.01 and M2-pH 4/0.1 samples did not completely inhibit the growth of *S. aureus*, as the OD of one of their inoculums exceeded 0.2 (Fig. 2(A)). However, the M2-pH 10/0.01, M2-pH 7/0.1, and M2-pH 10/0.1 samples maintained good antibacterial activity. At the same time, the inhibition zones around M2-pH 10/0.01, M2-pH 7/0.1, and M2-pH 10/0.1 were still clearly visible, although the sizes were reduced (Fig. S4). For M4-pH 10/0.01 and M4-pH 7/0.1, the OD values of the inoculums increased, while M4-pH 10/0.1 presented the best antibacterial property. In addition, the ZOI experiment showed that only M4-pH 10/0.1 produced an inhibition zone around the sample, while the zones around the other samples disappeared, indicating that mineralization inevitably reduced the antibacterial activity of the AgNP-loaded coatings and that only the pH 10/0.1 group maintained sufficient activity after four days of immersion in SBF.

To further investigate the antibacterial activity of these surfaces, spread plate assays were performed. *S. aureus* at a concentration of 10^5 CFU/mL was cultured on the specimens for 12 h and spread on agar for colony counting. The results in Fig. 2(C) indicate that bacteria substantially accumulated on Ti, pTi, and pTi-DA. Conversely, the *S. aureus* colonies on AgNPs evidently declined; only a few colonies formed on the plates of pH 10/0.01 and pH 7/0.1, and the pH 10/0.1 contained nothing, which agreed well with the results of the ZOI assay. After 2 or 4 days of mineralization, the antibacterial properties of all groups significantly decreased, with the exception of the pH 10/0.1 group.

The live/dead assay allows the living and dead bacteria to be visualized based on the colour change during the experiment. In this assay, SYTO 9 and PI were used to stain living and dead cells, respectively; SYTO 9 penetrates the cell membrane of both living and dead bacteria and presents green fluorescence, while PI can only penetrate the cell membrane of dead bacteria and emits red fluorescence. Therefore, samples without antibacterial properties

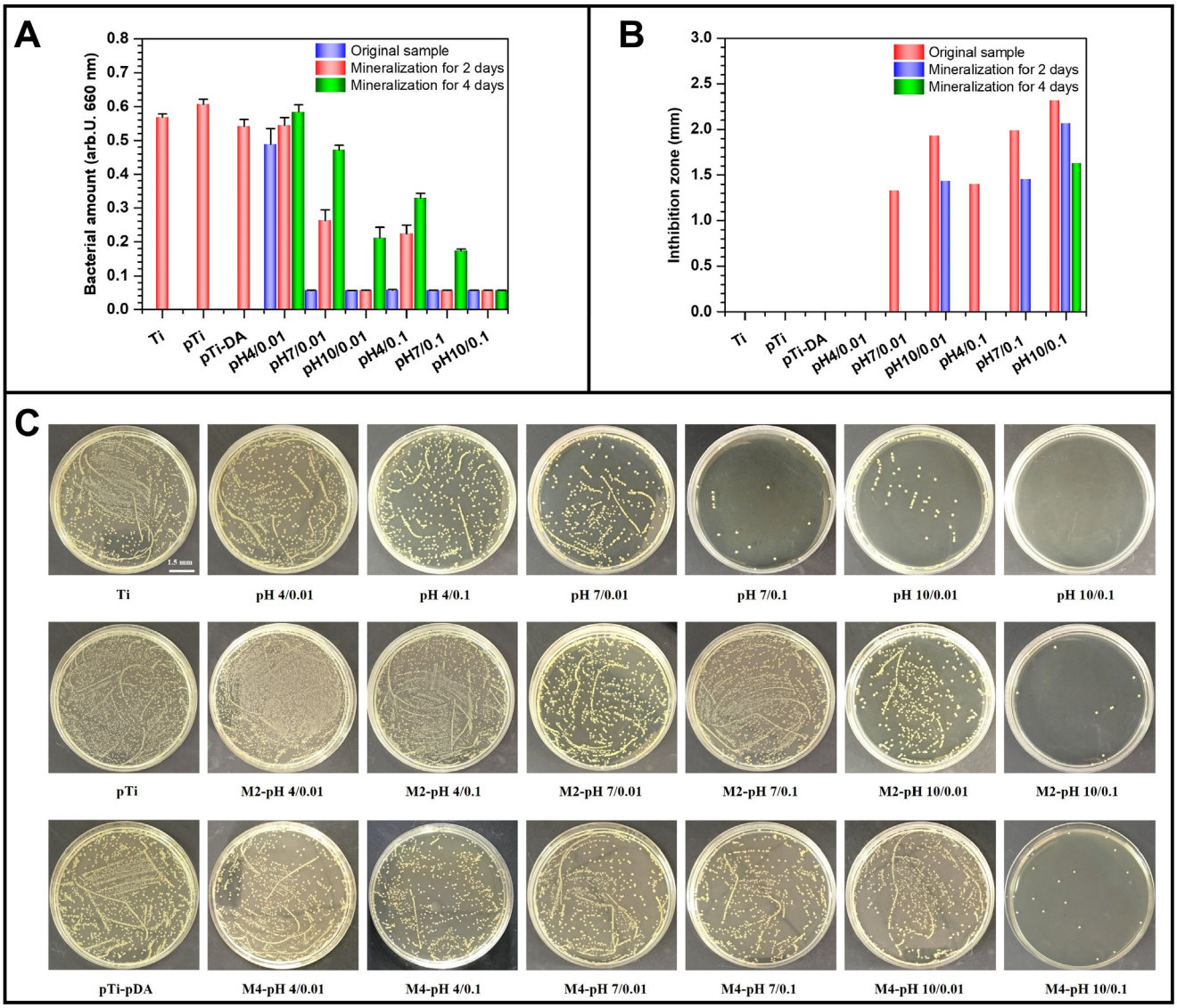

Fig. 2. Evaluation of the antibacterial activity of AgNP-loaded coatings. (A) Bacterial quantity in the inoculum after incubation on Ti-, pore Ti-, pDA-coated porous Ti-, and AgNP-modified porous Ti for 6 h. (B) The diameter of the inhibition zone around Ti, pore Ti, pDA-coated porous Ti, AgNP-modified porous Ti and sample mineralization for 2 and 4 days. (C) Antibacterial properties of Ti, porous Ti, pDA-coated porous Ti, and AgNP-modified porous Ti after mineralization for 0, 2, and 4 days determined by agar plating.

should be covered with green (live) bacteria, those with moderate antibacterial properties should be covered with green and red (dead) bacteria, and samples with potent antibacterial properties should have neither since the powerful antibacterial specimens kills the microbe at the first encounter and prevents adhesion [49].

As shown in Fig. S5, the antibacterial properties of these AgNPs display a positive correlation trend with the amount of AgNPs in the samples. Specifically, rapid and extensive adhesion of *S. aureus* occurred on the surfaces of Ti, pTi, and pTi-DA. Few bacteria adhered to the AgNP-loaded surface, and the percentage of dead cells was higher than that on the control. Microbial adhesion on the surfaces of pH 7/0.01 and pH 4/0.1 was suppressed to 20% and 15%, respectively, compared to that of Ti. Few bacteria were observed on the surfaces of pH 10/0.01, pH 7/0.1, and pH 10/0.1, which exhibited the highest antibacterial ability of these coatings. After mineralization for 2 days, biofilms and an increased quantity of bacteria were observed on the M2-pH 4/0.01, M2-pH 4/0.1, and M2-pH 7/0.01 surfaces, while few bacteria were seen on the sur-

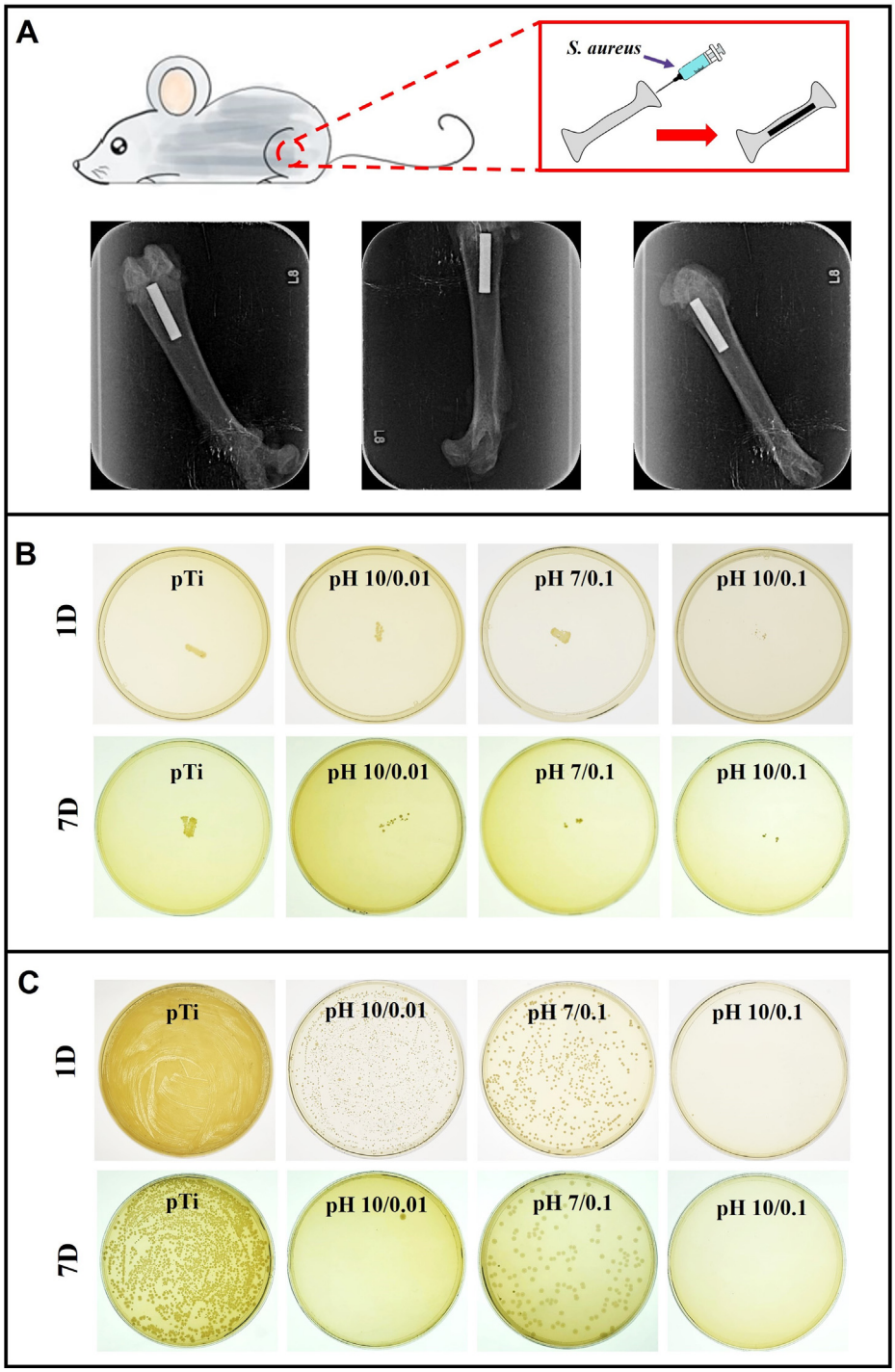

Fig. 3. In vivo antibacterial assay of AgNP-loaded coatings. (A) Scheme of the *in vivo* antibacterial assay. (B) X-ray images of the femurs with the implants. (C) Roll-over cultures of samples after 1 day and 7 days implantation. (D) *S. aureus* re-cultures on agar after dissociation from the embedded samples after implantation for 1 day and 7 days.

faces of M2-pH 10/0.01 and M2-pH 10/0.1, which illustrates that the samples with more AgNPs possess better antibacterial activity. After 4 days of mineralization, all samples except M4-pH 10/0.1 displayed general antibacterial properties, as their surfaces were covered by dead bacteria, whereas nothing was seen on the M4-pH 10/0.1 surface, indicating a long-term antibacterial ability.

To further study how long the antibacterial effect persists, further antibacterial tests with the spread plate method and live/dead staining of group pH 10/0.1 were performed after 5 and 7 days of SBF immersion. Fig. S6(A) shows that almost no bacteria were on the surface of M5-pH 10/0.1 compared with the widely adhered live (stained green) bacteria on the pTi-DA surface, while a large number of bacteria was observed on the surface of M7-pH 10/0.1, but most of them lost vitality. In the bacterial re-culture results (Fig. S6(B)), active bacteria on the surface of pTi-DA were densely distributed on the plate. Few viable bacteria were observed on the M5-pH 10/0.1 plate, while the number of vital bacteria on the surface of M7-pH 10/0.1 was increased compared to that of M5-pH 10/0.1. Therefore, as the results showed, the pH 10/0.1 group has acceptable antibacterial activity in simulated body fluids that can be maintained for at least 7 days.

2.3. In vivo antibacterial assay of AgNPs loaded coatings

To further determine the antibacterial ability of these AgNP-loaded coatings *in vivo*, a rat model was developed with bacterial

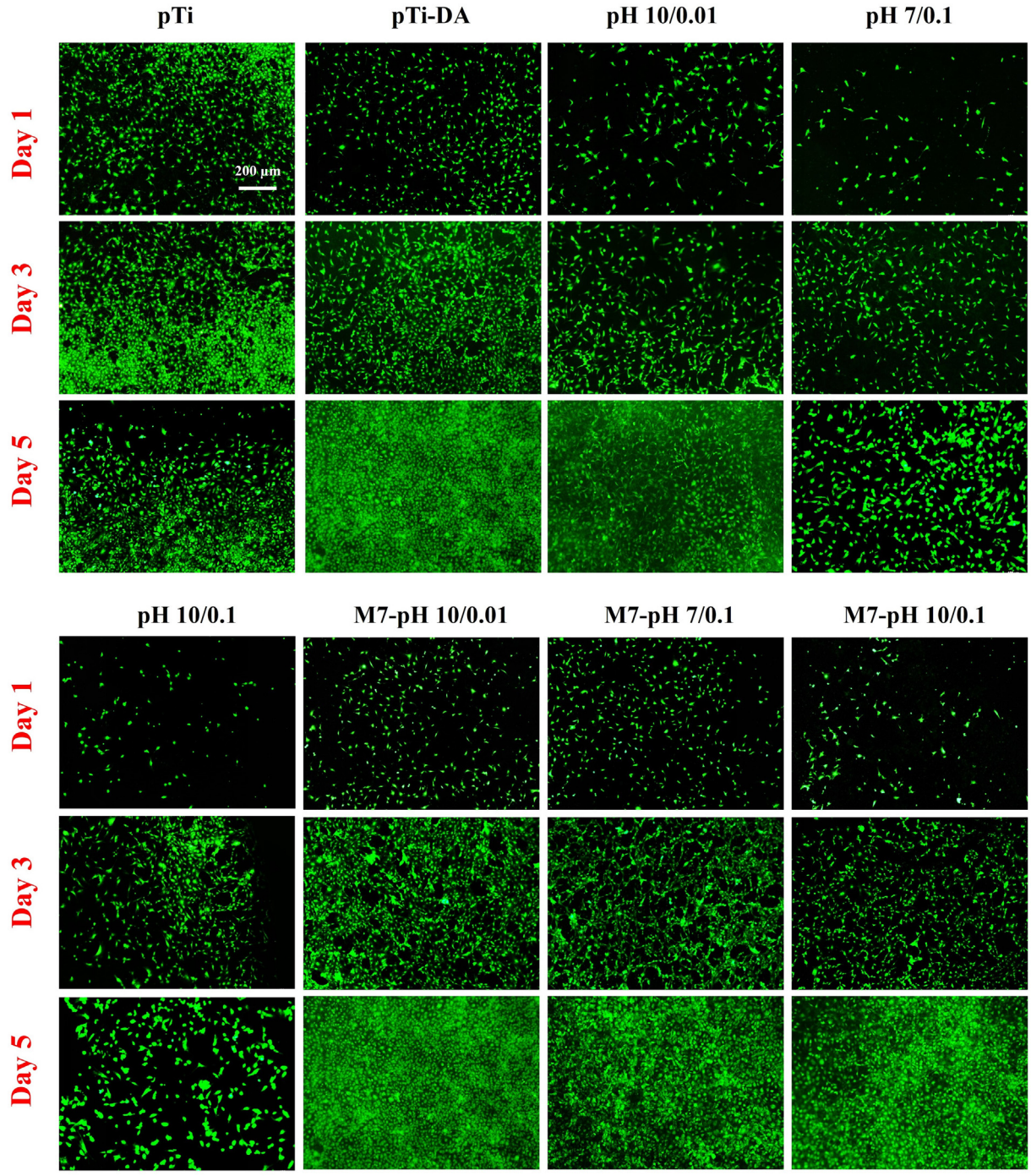

Fig. 4. Rhodamine 123 staining of MC 3 T3-E1 fibroblasts on various samples.

injection in the femoral medullary cavity (Fig. 3(A)). X-ray images of the animal model are depicted in Fig. 3(B) Specimens were inserted in the medullary cavity after the injection of an *S. aureus* suspension. After 1 and 7 days of implantation, the samples were removed for further analysis. Roll-over cultures were conducted, and the results are shown in Fig. 3(C): Massive bacteria were observed on the Ti rod, whereas the bacteria on the AgNP-modified rod were inhibited or killed, and the *S. aureus* colonies were sporadic compared to those of pTi. AgNP-modified Ti rods maintained their antibacterial ability after implantation for 1 and 7 days. To further verify the roll-over result, bacteria were detached from the rod and re-cultured on an agar plate. As shown in Fig. 3(D), massive bacterial colonies were observed on the agar plate of the pTi group, while colonies of the AgNP-loaded groups were significantly less than those on pTi, indicating that these AgNP-modified coatings possessed *in vivo* antibacterial activity. The antibacterial ability can be characterized by the number of colonies on the agar plate, as shown in Fig. 3(D). Obviously, the pH 10/0.1 sample possessed the strongest antibacterial activity, followed by pH 10/0.01, whereas pH 7/0.1 was the worst. As expected, the number of bacteria was reduced after 7 days of implantation in contrast to the 1 day of implantation that occurs due to tissue repair and the immune response.

2.4. Biocompatibility of AgNPs loaded coatings

Since the pH 10/0.01, pH 7/0.1, and pH 10/0.1 samples displayed better antibacterial effects in the antibacterial evaluations, we selected these three groups to assess osteoblast compatibility. As shown in the fluorescence images in Fig. 4, after one day of culture, the quantities and spreading behaviour of cells was better on the Ti, pTi, and pTi-DA than the AgNP-modified surfaces. After 3 days of culture, fewer cells adhered to the pH 10/0.01, pH 7/0.1, and pH 10/0.1 coatings than to the Ti, pTi, and pTi-DA coatings, but the number of cells increased, which confirmed their biosafety to some extent. After 7 days of mineralization, the M7-pH 10/0.1 group showed better cytocompatibility than the pH 10/0.1 group. This corresponds to the physiological requirements in the early implantation stage, where anti-infection is more important, and tissue repair holds a more significant position in the later period. Similar phenomena were observed in the 5-day cell culture, and the cells on mineralized samples had the best growth behaviour and were similar to the control. The amount and even growth rate of cells on pH 10/0.1 increased, further confirming the biosafety of these AgNP-loaded surfaces. The results of the MTT assay (Fig. S7) were in accordance with the fluorescence results, which verified the exceptional biocompatibility of pH 10/0.1.

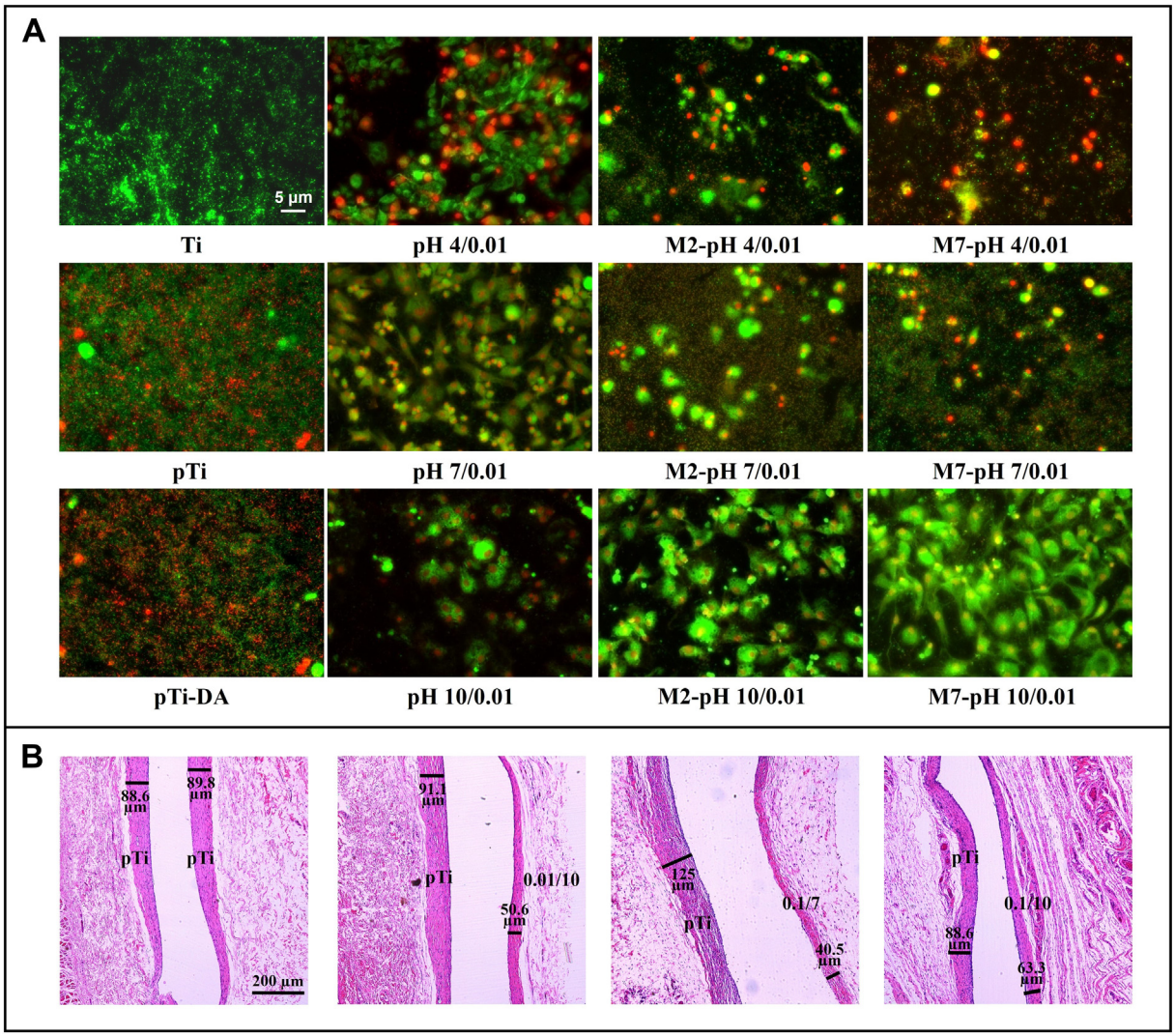

Fig. 5. Co-culture of bacterial and cell or tissue. (A) Live/dead staining of fibroblasts and *S. aureus* on various surfaces. (B) HE staining of local tissue (pretreated with *S. aureus*) around different samples after 1 month of subcutaneous implantation.

2.5. Co-culture of bacterial with cell and tissue

Dental implants are used in a physiological environment where cells and microbes coexist, and they require antibacterial properties [50]. Therefore, the co-culture of bacteria with cells was performed to evaluate the biological effect of antibacterial implants in complex environments. As the fluorescence images show in Fig. 5(A), massive bacterial colonies adhered to the Ti, pTi, and pDA implants, while only a few MC3T3-E1 cells were observed due to the overgrowth of bacteria. In contrast, more live cells

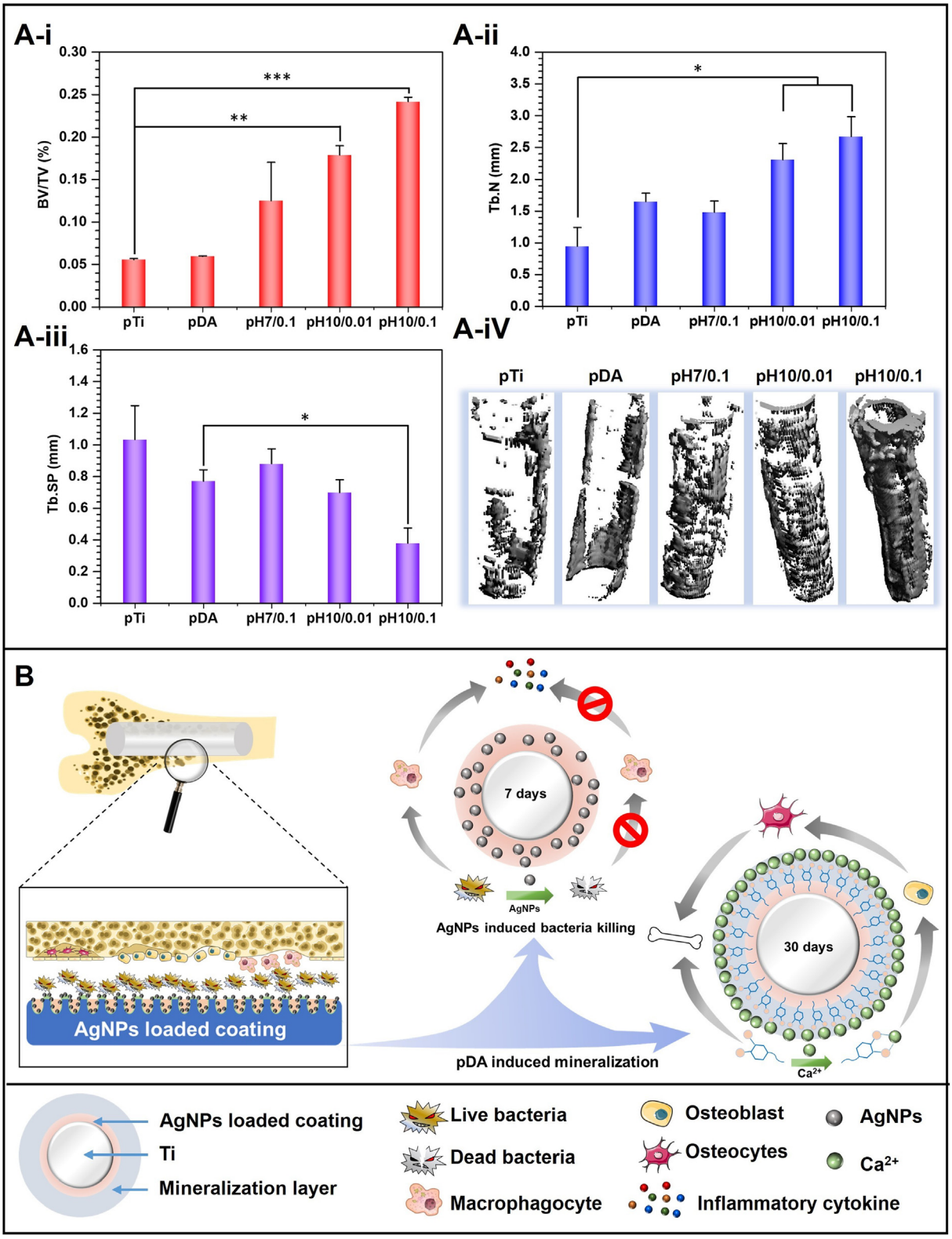

Fig. 6. 3D micro-CT modelling of porous various samples. (Ai–Aiii) Quantitative assessment of new bone surrounding the implant according to the percentage of bone to tissue volume (BV/TV), Tb. N and Tb. SP value and A-iV) 3D micro-CT reconstructed images. (B) Schematic illustration of the induced osteogenesis supposal. Data were expressed as the mean ± SD, n = 3. Statistically significant differences are indicated by *p < 0.05, **p < 0.01 or *** p < 0.001 compared with porous Ti.

adhered to samples that possessed moderate antibacterial behaviour, since antibacterial samples inhibit the proliferation of microbes, which favours cell growth. It is well known that the antibacterial property of these AgNP-loaded surfaces is associated with cytotoxicity, so the cell viability in the bacterial infection environment is determined by a balance of antibacterial activity and cytotoxicity. As displayed in Fig. 5(A), two- and seven-day mineralization of pH 10/0.01 and pH 7/0.1 (M2 and M7) caused a decrease in live 3 T3 fibroblasts on the surfaces since the AgNPs were partly covered by the mineralized layer. For the pH 10/0.1 group, even though the antibacterial ability was diminished as mineralization proceeded, the inhibitory effect of AgNPs on the cells was also decreased. As shown in Fig. 5, no bacteria were observed on pH 10/0.01 after 7 days of mineralization; moreover, the cells spread well, which indicates that the M7-pH 10/0.1 group possesses the proper antibacterial capacity to maintain the balance of the cell/bacteria co-exit environment.

Furthermore, the tissue response of pTi, 10/0.01, and pH 7/0.1, 10/0.01 samples with bacterial injections was determined after subcutaneous implantation in SD rats. After implantation for 1 month, the tissue around the implants was harvested and HE was stained for histological analysis. As shown in Fig. 5(B), fibrous capsules, which are signs of tissue inflammation, were formed. Therein, the capsule around pTi was thickest, whereas the AgNP-loaded samples tended to prevent capsule formation. Since the implantation-induced capsule was associated with tissue response, the results revealed that the AgNPs did not cause severe inflammation. Moreover, their antibacterial properties could inhibit the initial inflammation caused by microorganisms, which makes these AgNP-loaded coatings promising candidates for implants used in infection sites.

After systemically evaluating the biological security of these AgNP-loaded surfaces, 3D micro-CT analysis was carried out to investigate bone regeneration under bacterial infection conditions. Prior to implantation, *S. aureus* inoculum was injected, and then Ti rods were implanted into the infected marrow cavity. According to the results of Fig. 6(A-i), Ti rods modified with pH 10/0.1 and pH 10/0.01 presented the highest percentage of bone to tissue volume (BV/TV), which may be due to their strongest antibacterial properties. Moreover, consistent with the BV/TV results, the increased trabecular number (Tb. N) and lower trabecular separation (Tb. SP) also demonstrated that pH 10/0.1 exhibited exceptional osteogenesis capacity. In contrast, as the 3D model of Fig. 6(A-iii) shows, serious bone loss occurred around the porous Ti- and pDA-modified Ti, which was incapable of antibacterial properties.

The gap between biomaterials and bone is a complex environment where bacteria, immunocytes and osteocytes intermingle [51,52]. The crosstalk signalling between the skeletal system and immune system has also been proven to dramatically influence the whole bone repair process [53]. Once biomaterials are implanted into bone, an immune response induced by foreign bodies and bacteria occurs immediately, which is an early-stage event associated with the inflammation and wound healing process [43]. Not considering the response induced by the foreign body, bacteria are the main factor that influences the local immune response. The inflammatory response caused by bacterial infection is initiated with groups of pathogens and bacterial lipopolysaccharides, and the uncontrollable inflammatory response leads to implant failure by a systemic defence reaction [54]. The *S. aureus* that was chosen to be injected into the marrow cavity is the most common pathogen in periprosthetic joint infections and stimulates immune cells, especially macrophages, to secrete inflammatory cytokines such as IL-1β, TNF-α, IFN-γ secretion and iNOS production, ultimately leading to a decrease in bone tissue regeneration [55–57]. Thus, implants with strong antibacterial ability can reduce the incidence rate of infection-related inflammation, which favours bone regeneration in some manners. AgNPs are recognized as important antibacterial materials due to their effective and broad inhibition of bacterial infection. Polydopamine with metal-binding and reduction abilities can induce Ag^+ to form AgNP coatings on various substrates and trigger mineralization.

Mineralization is a spontaneous process that occurs in pDA-modified implants *in vivo*, and it inevitably decreases the antibacterial property while increasing the cytocompatibility to a certain degree. As such, when an implant is first inserted, these AgNP-exposed surfaces play the main role of bacterial killing and inhibiting bacteria-induced inflammation. As mineralization proceeds, the antibacterial effect reduces, and the cytocompatibility of these surfaces simultaneously improves. At this period, approximately one week after implantation, the main demands of the issue change. Tissue regeneration is the most important factor; thus, phenolic hydroxyl groups that can chelate Ca^{2+} to trigger mineralization are the main factors [58]. Therefore, it can be concluded that the pDA-induced AgNPs could function throughout the whole implantation stage. The antimicrobial activity of AgNPs is most important aspect in the first stage of implantation, whereas the phenolic hydroxyl groups that can trigger mineralization promote tissue repair in the later stages of implantation.

3. Conclusions

AgNPs with a uniform distribution were successfully prepared on porous Ti surfaces by pDA-induced reduction. We proposed and proved that the amount and morphology of AgNPs can be controlled by adjusting the feeding concentration and pH of the silver nitrate solution. An alkaline environment and a high concentration of silver nitrate were more conducive to generating AgNPs and endowed Ti with better antibacterial properties. The AgNP-loaded surface formed at pH 10 and a feeding concentration of silver nitrate 0.1 mg/mL possessed the most potent antibacterial activity. Mineralization of the samples was carried out by immersion in SBF for up to one week; after mineralization, the antibacterial activity of these coatings decreased, while their cytocompatibility was remarkably improved. Implantation experiments revealed that these AgNP-loaded coatings function well *in vivo*, and the tissue response in a bacteria-exposed environment shows that the AgNPs on these coatings significantly prevent the inflammation caused by microbes.

In conclusion, AgNP-loaded coatings with various antibacterial abilities can be obtained by adjusting pH and feeding concentration of the silver nitrate solution; *in vitro* and *in vivo* study showed the favourable cell- and tissue-compatibility by subsequent mineralization after implantation. The combined antibacterial property and well biocompatibility endowed this strategy with great significance for clinical applications.

4. Experimental

4.1. Materials

Commercial pure titanium (Ti) was purchased from Baoji Nonferrous Metal Co., Ltd. (Shanxi Province, China). Dopamine, silver nitrate, $CaCl_2 \times 2\ H_2O$, KH_2PO_4, NaCl, NaOH, Tris base, MTT, and rhodamine 123 were purchased from Sigma-Aldrich. Foetal bovine serum and α-minimum Eagle's medium were purchased from Gibco. *Staphylococcus aureus* (*S. aureus*) and the murine fibroblast cell line MC3T3-E1 were obtained from ATCC. Other reagents were purchased from Sinopharm Chemical Reagent Co., Ltd.

Four-week-old SD rats (male, approximately 200 g) were obtained from the Experimental Animal Department of Anhui Medical University (AHMU). All animal experimental methods

were approved by the ethical committee of the AHMU, and all animal experiments were performed in accordance with the guidelines of the AHMU.

4.2. Preparation of the AgNPs loaded coatings

Pure titanium discs were mechanically polished up to 2000 grit and then ultrasonically cleaned with acetone, ethanol, and deionized water sequentially. After soaking for 12 h in 5 M NaOH solution at 60℃, the titanium pieces were boiled with 100℃ deionized water for 2 h and denoted as pTi (porous titanium). These titanium discs were immersed in a 2 mg/mL dopamine solution (pH 8.5) for 24 h at room temperature and designated pTi-DA. Then, the pTi-DA was immersed in silver nitrate (0.01 mg/ml, 0.1 mg/ml) solutions of pH 4, 7 and 10 for 1 h at room temperature, which were denoted as pH 4/0.01, pH 7/0.01, pH 10/0.01, pH 4/0.1, pH 7/0.1 and pH 10/0.1, respectively.

4.3. Characterization of the AgNPs loaded coatings

The surface morphologies of pTi and modified Ti were characterized by scanning electron microscopy (SEM), and the surface composition was determined by X-ray photoelectron spectroscopy (XPS). Water contact angle (WCA) analysis was performed with deionized water at room temperature using a drop shape analysis system (DSA 100), and five samples in each group were measured twice. For mineralization, each specimen was soaked for two months at 37℃ in phosphate buffered saline (PBS), which was collected at predetermined intervals and replaced with a fresh sample for mineralization. To further investigate the reaction mechanism, surface plasmon resonance spectroscopy (SPR) was performed. Twenty microlitres of dopamine solution (2 mg/mL) was added to 2 mL of silver nitrate (0.01 mg/ml, 0.1 mg/ml) solution at pH 4, 7 and 10, and the SPR was monitored via a UV–Vis spectrophotometer.

The synthesis of the nano-silver process on the gold-plated chip with a pre-deposited polydopamine film was determined by QCM-D technology in real time. The QCM-D wafer was immersed in a 2 mg/mL dopamine solution at 37 °C for 24 h, and then the QCM-D chip with the polydopamine film was cleaned and installed in the QCM instrument. During the test, deionized water with the same pH of the test solution was introduced until the frequency F reached a constant value. Then, a silver nitrate solution with a certain concentration and pH value was continuously injected, AgNPs were formed with decreasing frequency, and deionized water with the same pH was injected when the solution reached a plateau to remove the weakly bonded AgNPs. The change in resonance frequency before and after the experiment is proportional to the change in the mass of the coating.

4.4. Mineralization of the coating in simulated body fluid (SBF)

Mineralization is a natural behaviour on pDA-modified surfaces after implantation; here, we use SBF as a substitute for interstitial fluid and to simulate the *in vivo* environment. The SBF (pH 7.4) was composed of 160 mM sodium chloride (NaCl), 4.22 mM sodium bicarbonate ($NaHCO_3$), 3.02 mM potassium chloride (KCl), 1.01 mM dipotassium hydrogen phosphate trihydrate ($K_2HPO_4 \cdot 3H_2O$), 1.52 mM magnesium chloride hexahydrate ($MgCl_2 \cdot 6H_2O$), 2.63 mM calcium chloride ($CaCl_2$), and 0.5 mM sodium sulfate (Na_2SO_4), and was buffered by 50 mM Tris. The samples were placed in 24-well plates and incubated with 1 mL SBF at 37 °C, and the solution was replenished daily. The samples were removed after one to seven days and rinsed with deionized water for 10 min. The samples were denoted M*n*-Ti, M*n*-pTi, M*n*-pTi-DA, M*n*-pH 4/0.01, M*n*-pH 7/0.01, M*n*-pH 10/0.01, M*n*-pH 4/0.1, M*n*-pH 7/0.1, and M*n*-pH 10/0.1, with *n* representing the incubation days.

4.5. Antibacterial assay

S. aureus was selected for the following bacterial evaluation as it is the main pathogenic bacteria of metallic implants. *S. aureus* was precultured in a brain heart infusion (BHI) for 24 h, and then it was adjusted to a concentration of 10^5 CFU/mL for the antibacterial assay. To simulate the early antibacterial properties of the coating to further study the antibacterial effect, the samples were immersed in SBF for 1, 2, 5, and 7 days. All samples were UV sterilized prior to the antibacterial experiments.

4.5.1. Inhibition of biofilm formation

The surface biofilms were analysed by the spread plate method. All samples were placed in 24-well plates after sterilization, and 1 mL of the bacterial suspension was added. After 12 h of static culture at 37 °C, the surviving bacteria on the samples were collected into a new Petri dish by three washes with PBS. Then, the eluted bacteria were diluted 10^5 times and cultured for 24 h on agar to count the colonies.

Live and dead bacteria were fluorescently stained to evaluate their viability. Samples were placed in a new 24-well plate and then immersed in the bacterial suspension at a concentration of 10^5 CFU/mL. After 24 h incubation, samples were stained with acridine orange and ethidium bromide, washed with sodium chloride and observed by fluorescence microscopy. Viable bacteria with intact cell membranes were stained green, whereas nonviable bacteria with damaged membranes were stained red.

The antibacterial rates (Ra) of adhered bacteria on the samples were calculated based on the following formulas:

$$(\mathrm{Ra})(\%) = (\mathrm{A} - \mathrm{B})/\mathrm{A} \times 100\%$$

where A indicating the average number of viable bacteria on Ti, pTi and pTi-DA, and B is the average number of viable bacteria on other specimens.

4.5.2. Antibacterial evaluation of the surrounding environment

The antibacterial activity on the surrounding environment was tested by the following methods: 1) 1 mL 10^5 CFU/mL bacterial solution was added to each well. After incubation at 37 °C for 24 h, 150 μL of bacterial suspension from each well was removed for optical density measurements at 660 nm (OD 660) using a microplate reader. 2) The bacterial solution was diluted with PBS at different multiples according to the turbidity. One hundred microlitres of the diluted solution was applied to each plate and cultured at 37 °C for 24 h. Then, the colonies were counted, and the original concentration was calculated. 3) The antibacterial effect of the samples on *S. aureus* in the surrounding system was determined by zone of inhibition (ZOI) tests. A 20 μL sample of the test strain solution with a bacterial density of 10^7 CFU/mL was uniformly spread onto an agar plate. The samples were placed face down on agar medium and cultured at 37 °C for 24 h, followed by measuring the ZOI diameters.

4.6. Cell morphology

The mouse osteoblastic cell line MC3T3-E1 was employed to assess cytotoxicity. Cells were cultured in α-MEM containing 10% foetal bovine serum (FBS) in a humidified atmosphere of 5% CO_2 at 37 °C. The sterilized samples were placed in 24-well plates on which the cells were seeded at a density of 1×10^5 cells/mL. A 600 μL cell suspension was added to each well, and the medium was refreshed every 2 days. After incubation for 1, 3, and 5 days in a cell incubator, loosely adherent cells were removed by gently rinsing three times with sterile PBS, and then the samples were transferred into 2.5% glutaraldehyde for 4 h for fixation. Subse-

quently, these specimens were stained with rhodamine 123 for 15 min and observed with a fluorescence microscope.

4.7. Evaluation of competitive bacterial-cell adhesion

As widely reported, a sort of "race for the surface" between cells and bacteria starts promptly after implantation [59]. Therefore, the competitive adhesion between bacterial and mammalian cells was evaluated to mimic the infection conditions. Eighty microlitres of bacterial suspension with a density of 10^6 CFU/mL was added to the surfaces of the samples and incubated at 37 °C for 4 h. Then, MC3T3-E1 cells at a density of 1×10^5 cells/mL were added to each well and cultured at 37 °C and 5% CO_2. After 24 h, live-dead bacterial staining was performed. The morphology and quantity of bacteria and cells were observed under a fluorescence microscope.

4.8. In vivo experiments

4.8.1. Subcutaneous implantation

Four-week-old SD rats were used in this study to evaluate the biological responses of the surrounding tissues towards Ti plates and AgNP-loaded samples. Briefly, 10 μL *S. aureus* suspensions standardized to 0.5 McFarland standards (10^8 CFU/mL) were added to the surfaces of the sterilized samples. The rats were anaesthetized by intraperitoneal injection of 1% pentobarbital prior to surgery; their backs were shaved, depilated, and disinfected with iodine. Then, a 10-mm longitudinal skin incision was made to expose the superficial layer of the deep fascia. Blunt dissection was performed with scissors to form a pocket in which the implant was inserted with the modified surface towards the skin. Finally, each subcutaneous pocket was sutured using a surgical thread. After 1 month, the animals were euthanized, and the plates with the surrounding tissues were harvested for further histological analysis.

4.8.2. Marrow cavity implantation

SD rats were anaesthetized by intraperitoneal injection of 1% pentobarbital. Both hind legs were shaved, depilated, and disinfected with iodine. After bonding to the operating table, the femoral condyles of both hind legs were exposed by skin incision, and a Kirschner wire (1.5 mm diameter) was used to drill a hole through the cortical and cancellous bone. A volume of 20 μL *S. aureus* suspension with a concentration of 10^3 cfu/mL was injected into the cavity, and sterile implants (2 mm in diameter and 8 mm in length) were inserted. After implantation, the hole was blocked by bone wax, and the wound was closed with a suture. After 1 and 7 days, the samples were explanted, rolled on nutrient agar plates, and immersed in 2.5 mL of BHI before being re-cultured on agar. After one day of culture on agar, photos of the re-cultured agar plate were taken.

4.9. Statistical analysis

Each test was repeated three times, and the results are expressed as the mean ± standard deviation. The data were tested for homogeneity and then assessed statistically using one-way ANOVA and a Student-Newman-Keuls (SNK) post hoc test. In the figures, statistically significant differences ($p < 0.05$) are denoted with an asterisk (*).

Ethical statement

All experimental protocols used in this research were approved by the Ethical Committee of by Anhui Medical University (protocol number: 20160126).

CRediT authorship contribution statement

Xiaowei Wang: Writing - original draft, Conceptualization, Data curation. **Kehui Xu:** Methodology, Writing - original draft, Formal analysis, Investigation. **Wendi Cui:** Writing - review & editing, Methodology. **Xi Yang:** Software, Visualization. **Manfred F. Maitz:** Supervision, Validation. **Wei Li:** Visualization, Validation. **Xiangyang Li:** Supervision, Resources, Funding acquisition. **Jialong Chen:** Conceptualization, Project administration, Funding acquisition.

Declaration of Competing Interest

The authors declare that they have no known competing financial interests or personal relationships that could have appeared to influence the work reported in this paper.

Acknowledgements

This work was supported by the National Natural Science Foundation of China (no. 31670967 and 32000932), the Scientific Research Foundation of the Institute for Translational Medicine of Anhui Province (no. 2017zhyx19), University Outstanding Youth Talent Support Program of Anhui Province (no. gxyq2018007) and Postdoctoral Science Foundation of Anhui Province (No. 2018B264).

Appendix A. Supplementary material

Supplementary data to this article can be found online at https://doi.org/10.1016/j.matdes.2021.109944.

References

[1] K. Pałka, R. Pokrowiecki, Porous titanium implants: a review, Adv. Eng. Mater. 20 (5) (2018) 1700648.
[2] S.E. Rossiter, M.H. Fletcher, W.M. Wuest, Natural products as platforms to overcome antibiotic resistance, Chem. Rev. 117 (19) (2017) 12415–12474.
[3] R. Laxminarayan, A. Duse, C. Wattal, A.K. Zaidi, H.F. Wertheim, N. Sumpradit, E. Vlieghe, G.L. Hara, I.M. Gould, H. Goossens, C. Greko, A.D. So, M. Bigdeli, G. Tomson, W. Woodhouse, E. Ombaka, A.Q. Peralta, F.N. Qamar, F. Mir, S. Kariuki, Z.A. Bhutta, A. Coates, R. Bergstrom, G.D. Wright, E.D. Brown, O. Cars, Antibiotic resistance-the need for global solutions, Lancet Infect. Dis. 13 (12) (2013) 1057–1098.
[4] X. Li, H. Bai, Y. Yang, J. Yoon, S. Wang, X. Zhang, Supramolecular antibacterial materials for combatting antibiotic resistance, Adv. Mater. 31 (5) (2019) e1805092.
[5] H. Chouirfa, H. Bouloussa, V. Migonney, C. Falentin-Daudre, Review of titanium surface modification techniques and coatings for antibacterial applications, Acta Biomater. 83 (2019) 37–54.
[6] P. Makvandi, R. Jamaledin, M. Jabbari, N. Nikfarjam, A. Borzacchiello, Antibacterial quaternary ammonium compounds in dental materials: a systematic review, Dent. Mater. 34 (6) (2018) 851–867.
[7] Q. Xin, H. Shah, A. Nawaz, W. Xie, M.Z. Akram, A. Batool, L. Tian, S.U. Jan, R. Boddula, B. Guo, Q. Liu, J.R. Gong, Antibacterial carbon-based nanomaterials, Adv. Mater. 31 (45) (2019) e1804838.
[8] M.L.W. Knetsch, L.H. Koole, New strategies in the development of antimicrobial coatings: the example of increasing usage of silver and silver nanoparticles, Polymers 3 (1) (2011) 340–366.
[9] G. Regea, Review on antibiotics resistance and its economic impacts, J. Pharmacol. Clin. Res. 5 (2018) 555675.
[10] Y. Yang, X. Wu, L. Ma, C. He, S. Cao, Y. Long, J. Huang, R.D. Rodriguez, C. Cheng, C. Zhao, L. Qiu, Bioinspired spiky peroxidase-mimics for localized bacterial capture and synergistic catalytic sterilization, Adv. Mater. 33 (8) (2021) e2005477.
[11] L. Ma, F. Jiang, X. Fan, L. Wang, C. He, M. Zhou, S. Li, H. Luo, C. Cheng, L. Qiu, Metal-organic-framework-engineered enzyme-mimetic catalysts, Adv. Mater. 32 (49) (2020) e2003065.
[12] W. Cheng, X. Zeng, H. Chen, Z. Li, W. Zeng, L. Mei, Y. Zhao, Versatile polydopamine platforms: synthesis and promising applications for surface modification and advanced nanomedicine, ACS Nano 13 (8) (2019) 8537–8565.
[13] N. Sanbhal, Y. Mao, G. Sun, R.F. Xu, Q. Zhang, L. Wang, Surface modification of polypropylene mesh devices with cyclodextrin via cold plasma for hernia repair: characterization and antibacterial properties, Appl. Surf. Sci. 439 (2018) 749–759.

[14] X. Zhang, G. Zhang, M. Chai, X. Yao, W. Chen, P.K. Chu, Synergistic antibacterial activity of physical-chemical multi-mechanism by TiO2 nanorod arrays for safe biofilm eradication on implant, Bioact. Mater. 6 (1) (2021) 12–25.
[15] Z. Lu, Y. Wu, Z. Cong, Y. Qian, X. Wu, N. Shao, Z. Qiao, H. Zhang, Y. She, K. Chen, H. Xiang, B. Sun, Q. Yu, Y. Yuan, H. Lin, M. Zhu, R. Liu, Effective and biocompatible antibacterial surfaces via facile synthesis and surface modification of peptide polymers, Bioact. Mater. 6 (12) (2021) 4531–4541.
[16] Y. Yang, X. Wu, C. He, J. Huang, S. Yin, M. Zhou, L. Ma, W. Zhao, L. Qiu, C. Cheng, C. Zhao, Metal-organic framework/Ag-based hybrid nanoagents for rapid and synergistic bacterial eradication, ACS Appl. Mater. Interfaces 12 (12) (2020) 13698–13708.
[17] B. Le Ouay, F. Stellacci, Antibacterial activity of silver nanoparticles: a surface science insight, Nano today 10 (3) (2015) 339–354.
[18] A. Panacek, M. Kolar, R. Vecerova, R. Prucek, J. Soukupova, V. Krystof, P. Hamal, R. Zboril, L. Kvitek, Antifungal activity of silver nanoparticles against Candida spp, Biomaterials 30 (31) (2009) 6333–6340.
[19] L. Zhao, H. Wang, K. Huo, L. Cui, W. Zhang, H. Ni, Y. Zhang, Z. Wu, P.K. Chu, Antibacterial nano-structured titania coating incorporated with silver nanoparticles, Biomaterials 32 (24) (2011) 5706–5716.
[20] A.A. Ivanova, M.A. Surmeneva, A.I. Tyurin, T.S. Pirozhkova, I.A. Shuvarin, O. Prymak, M. Epple, M.V. Chaikina, R.A. Surmenev, Fabrication and physico-mechanical properties of thin magnetron sputter deposited silver-containing hydroxyapatite films, Appl. Surf. Sci. 360 (2016) 929–935.
[21] S.S. Bayram, O.K. Zahr, J. Del Re, A.S. Blum, Nanoring formation via in situ photoreduction of silver on a virus scaffold, Nanotechnology 27 (48) (2016) 485603.
[22] H. Qin, H. Cao, Y. Zhao, C. Zhu, T. Cheng, Q. Wang, X. Peng, M. Cheng, J. Wang, G. Jin, Y. Jiang, X. Zhang, X. Liu, P.K. Chu, In vitro and in vivo anti-biofilm effects of silver nanoparticles immobilized on titanium, Biomaterials 35 (33) (2014) 9114–9125.
[23] M.C. Moulton, L.K. Braydich-Stolle, M.N. Nadagouda, S. Kunzelman, S.M. Hussain, R.S. Varma, Synthesis, characterization and biocompatibility of "green" synthesized silver nanoparticles using tea polyphenols, Nanoscale 2 (5) (2010) 763–770.
[24] M.S. Islam, N. Akter, M.M. Rahman, C. Shi, M.T. Islam, H.B. Zeng, M.S. Azam, Mussel-inspired immobilization of silver nanoparticles toward antimicrobial cellulose paper, ACS Sustain. Chem. Eng. 6 (7) (2018) 9178–9188.
[25] Y. Yang, P. Gao, J. Wang, Q. Tu, L. Bai, K. Xiong, H. Qiu, X. Zhao, M.F. Maitz, H. Wang, X. Li, Q. Zhao, Y. Xiao, N. Huang, Z. Yang, Endothelium-mimicking multifunctional coating modified cardiovascular stents via a stepwise metal-catechol-(amine) surface engineering strategy, Research (Wash D C) 2020 (2020) 9203906.
[26] X. Chen, Y. Gao, Y. Wang, G. Pan, Mussel-inspired peptide mimicking: an emerging strategy for surface bioengineering of medical implants, Smart Mater. Med. 2 (2021) 26–37.
[27] P. Gao, H. Qiu, K. Xiong, X. Li, Q. Tu, H. Wang, N. Lyu, X. Chen, N. Huang, Z. Yang, Metal-catechol-(amine) networks for surface synergistic catalytic modi fi cation: therapeutic gas generation and biomolecule grafting, Biomaterials 248 (2020) 119981.
[28] H. Lee, S.M. Dellatore, W.M. Miller, P.B. Messersmith, Mussel-inspired surface chemistry for multifunctional coatings, Science 318 (5849) (2007) 426–430.
[29] Z. Yang, X. Zhao, R. Hao, Q. Tu, X. Tian, Y. Xiao, K. Xiong, M. Wang, Y. Feng, N. Huang, G. Pan, Bioclickable and mussel adhesive peptide mimics for engineering vascular stent surfaces, Proc. Natl. Acad. Sci. USA 117 (28) (2020) 16127–16137.
[30] Y. Liu, K. Ai, L. Lu, Polydopamine and its derivative materials: synthesis and promising applications in energy, environmental, and biomedical fields, Chem. Rev. 114 (9) (2014) 5057–5115.
[31] Z. Wang, Y. Zou, Y. Li, Y. Cheng, Metal-containing polydopamine nanomaterials: catalysis, energy, and theranostics, Small 16 (18) (2020) e1907042.
[32] C. Guo, W. Cui, X. Wang, X. Lu, L. Zhang, X. Li, W. Li, W. Zhang, J. Chen, Poly-l-lysine/sodium alginate coating loading nanosilver for improving the antibacterial effect and inducing mineralization of dental implants, ACS Omega 5 (18) (2020) 10562–10571.
[33] Z.Y. Wang, M. Xing, O. Ojo, Mussel-inspired ultrathin film on oxidized Ti-6Al-4V surface for enhanced BMSC activities and antibacterial capability, RSC Adv. 4 (99) (2014) 55790–55799.
[34] T.S. Sileika, H.D. Kim, P. Maniak, P.B. Messersmith, Antibacterial performance of polydopamine-modified polymer surfaces containing passive and active components, ACS Appl. Mater. Interfaces 3 (12) (2011) 4602–4610.
[35] Y.J. Xie, L.N. Yue, Y.D. Zheng, L. Zhao, C.Y. Liang, W. He, Z.W. Liu, Y. Sun, Y.Y. Yang, The antibacterial stability of poly(dopamine) in-situ reduction and chelation nano-Ag based on bacterial cellulose network template, Appl. Surf. Sci. 491 (2019) 383–394.
[36] P.V. AshaRani, G. Low Kah Mun, M.P. Hande, S. Valiyaveettil, Cytotoxicity and genotoxicity of silver nanoparticles in human cells, ACS Nano 3(2) (2009) 279–290.
[37] E.I. Hassanen, A.A. Khalaf, A.F. Tohamy, E.R. Mohammed, K.Y. Farroh, Toxicopathological and immunological studies on different concentrations of chitosan-coated silver nanoparticles in rats, Int. J. Nanomedicine 14 (2019) 4723–4739.
[38] L. Rizzello, P.P. Pompa, Nanosilver-based antibacterial drugs and devices: mechanisms, methodological drawbacks, and guidelines, Chem. Soc. Rev. 43 (5) (2014) 1501–1518.
[39] J.R. Morones, J.L. Elechiguerra, A. Camacho, K. Holt, J.B. Kouri, J.T. Ramirez, M.J. Yacaman, The bactericidal effect of silver nanoparticles, Nanotechnology 16 (10) (2005) 2346–2353.
[40] M.V. Park, A.M. Neigh, J.P. Vermeulen, L.J. de la Fonteyne, H.W. Verharen, J.J. Briede, H. van Loveren, W.H. de Jong, The effect of particle size on the cytotoxicity, inflammation, developmental toxicity and genotoxicity of silver nanoparticles, Biomaterials 32 (36) (2011) 9810–9817.
[41] T.H. Kim, M. Kim, H.S. Park, U.S. Shin, M.S. Gong, H.W. Kim, Size-dependent cellular toxicity of silver nanoparticles, J. Biomed. Mater. Res. A 100 (4) (2012) 1033–1043.
[42] L. Pauksch, S. Hartmann, M. Rohnke, G. Szalay, V. Alt, R. Schnettler, K.S. Lips, Biocompatibility of silver nanoparticles and silver ions in primary human mesenchymal stem cells and osteoblasts, Acta Biomater. 10 (1) (2014) 439–449.
[43] D. Zhang, Q. Chen, C. Shi, M. Chen, K. Ma, J. Wan, R. Liu, Dealing with the foreign-body response to implanted biomaterials: strategies and applications of new materials, Adv. Funct. Mater. 31 (6) (2020) 2007226.
[44] Y. Xiao, W. Wang, X. Tian, X. Tan, T. Yang, P. Gao, K. Xiong, Q. Tu, M. Wang, M.F. Maitz, N. Huang, G. Pan, Z. Yang, A versatile surface bioengineering strategy based on mussel-inspired and bioclickable peptide mimic, Research (Wash D C) 2020 (2020) 7236946.
[45] Y. Yang, Y.Y. Deng, J.B. Huang, X. Fan, C. Cheng, C.X. Nie, L. Ma, W.F. Zhao, C.S. Zhao, Size-transformable metal-organic framework-derived nanocarbons for localized chemo-photothermal bacterial ablation and wound disinfection, Adv. Funct. Mater. 29 (33) (2019) 1900143.
[46] X. Fan, F. Yang, J. Huang, Y. Yang, C. Nie, W. Zhao, L. Ma, C. Cheng, C. Zhao, R. Haag, Metal-organic-framework-derived 2D carbon nanosheets for localized multiple bacterial eradication and augmented anti-infective therapy, Nano Lett. 19 (9) (2019) 5885–5896.
[47] H.Y. Jung, I.S. Yeo, T.U. Kim, H.C. Ki, H.B. Gu, Surface plasmon resonance effect of silver nanoparticles on a TiO2 electrode for dye-sensitized solar cells, Appl. Surf. Sci. 432 (2018) 266–271.
[48] G. Jin, H. Qin, H. Cao, S. Qian, Y. Zhao, X. Peng, X. Zhang, X. Liu, P.K. Chu, Synergistic effects of dual Zn/Ag ion implantation in osteogenic activity and antibacterial ability of titanium, Biomaterials 35 (27) (2014) 7699–7713.
[49] S. Mei, H. Wang, W. Wang, L. Tong, H. Pan, C. Ruan, Q. Ma, M. Liu, H. Yang, L. Zhang, Y. Cheng, Y. Zhang, L. Zhao, P.K. Chu, Antibacterial effects and biocompatibility of titanium surfaces with graded silver incorporation in titania nanotubes, Biomaterials 35 (14) (2014) 4255–4265.
[50] R. Rasouli, A. Barhoum, H. Uludag, A review of nanostructured surfaces and materials for dental implants: surface coating, patterning and functionalization for improved performance, Biomater. Sci. 6 (6) (2018) 1312–1338.
[51] J. Lee, H. Byun, S.K. Madhurakkat Perikamana, S. Lee, H. Shin, Current Advances in Immunomodulatory Biomaterials for Bone Regeneration, Adv. Healthc. Mater. 8 (4) (2019) e1801106.
[52] Y. Xia, X. Fan, H. Yang, L. Li, C. He, C. Cheng, R. Haag, ZnO/nanocarbons-modified fibrous scaffolds for stem cell-based osteogenic differentiation, Small 16 (38) (2020) e2003010.
[53] C. Schlundt, H. Schell, S.B. Goodman, G. Vunjak-Novakovic, G.N. Duda, K. Schmidt-Bleek, Immune modulation as a therapeutic strategy in bone regeneration, J. Exp. Orthop. 2 (1) (2015) 1.
[54] H. Kumar, T. Kawai, S. Akira, Pathogen recognition by the innate immune system, Int. Rev. Immunol. 30 (1) (2011) 16–34.
[55] K.M. Rigby, F.R. DeLeo, Neutrophils in innate host defense against Staphylococcus aureus infections, Semin. Immunopathol. 34 (2) (2012) 237–259.
[56] C.M. Gries, T. Kielian, Staphylococcal biofilms and immune polarization during prosthetic joint infection, J. Am. Acad. Orthop. Surg. 25 (Suppl 1) (2017) S20–S24.
[57] T.D. Scherr, C.E. Heim, J.M. Morrison, T. Kielian, Hiding in plain sight: interplay between staphylococcal biofilms and host immunity, Front. Immunol. 5 (2014) 37.
[58] J.E. Mooney, B.E. Rolfe, G.W. Osborne, D.P. Sester, N. van Rooijen, G.R. Campbell, D.A. Hume, J.H. Campbell, Cellular plasticity of inflammatory myeloid cells in the peritoneal foreign body response, Am. J. Pathol. 176 (1) (2010) 369–380.
[59] C.R. Arciola, D. Campoccia, P. Speziale, L. Montanaro, J.W. Costerton, Biofilm formation in Staphylococcus implant infections. A review of molecular mechanisms and implications for biofilm-resistant materials, Biomaterials 33 (26) (2012) 5967–5982.